

Transmission of 32-Tb/s Capacity Over 580 km Using RZ-Shaped PDM-8QAM Modulation Format and Cascaded Multimodulus Blind Equalization Algorithm

Xiang Zhou, *Senior Member, IEEE*, Jianjun Yu, *Senior Member, IEEE*, Ming-Fang Huang, Yin Shao, Ting Wang, Peter Magill, Milorad Cvijetic, Lynn Nelson, Martin Birk, *Senior Member, IEEE*, Guodong Zhang, S. Ten, H. B. Matthew, and S. K. Mishra

Abstract—In this paper, we propose a novel synthesizing method for high-speed 8-ary quadratic-amplitude modulation (QAM) optical signal generation using commercial optical modulators with binary electrical driving signals. Using this method, we successfully generated 114-Gb/s pulse-duration modulation (PDM)-8QAM optical signals. Intradyne detection of PDM-8QAM optical signals with robust blind polarization demultiplexing has been demonstrated by using a new cascaded multimodulus equalization algorithm. With return-to-zero-shaped PDM-8QAM modulation and the proposed blind polarization demultiplexing algorithm, we demonstrate transmission of a record 32-Tb/s fiber capacity (320×114 Gb/s) over 580 km of ultralow-loss single-mode fiber-28 fiber by utilizing C + L-band erbium-doped fiber-amplifier-only optical amplification and single-ended coherent detection technique at an information spectral efficiency of 4.0 bit/s-Hz.

Index Terms—8-phase-shift keying (PSK), coherent, digital, fiber, modulation format, optical transmission, spectral efficiency.

I. INTRODUCTION

INCREASING the capacity that can be delivered over a single fiber has been historically proven to be the most cost-effective method to meet the need of ever growing demand in the core transport network. The 1990s breakthroughs in dense wavelength-division-multiplexing (DWDM) and erbium-doped fiber amplifier (EDFA) technologies have resulted in dramatic capacity increase by using simple ON/OFF key modulation format and direct intensity detection up to 10-Gb/s per wavelength. To further increase the capacity and lower the cost per transmitted bit, more spectrally efficient modulation/detection and Raman optical amplification techniques have been extensively investigated at higher data rates [1]–[34]. Until

now, the highest fiber capacity demonstrated in a transmission experiment was 25.6 Tb/s [5], where a C + L-band 160×160 Gb/s DWDM signal on a 50 GHz grid was transmitted over 240 km of standard single-mode fiber (SMF)-28 (SSMF) by using polarization-division-multiplexed (PDM), return-to-zero (RZ) differential quadrature phase-shift keying (DQPSK) modulation, delay-interferometer-based balanced detection, and hybrid EDFA/Raman optical amplification.

Recent progress in digital coherent detection technology has made possible the practical implementation of more sophisticated multilevel and multidimensional modulation formats, thereby opening a new avenue for further increasing the fiber capacity. Employing 64-ary PDM-RZ-8PSK modulation and single-ended digital coherent detection, we recently demonstrated 17-Tb/s (161×114 -Gb/s) transmission over 662 km of ultralow-loss (ULL) SMF-28 fiber using C-band EDFA amplification only [25]. Utilizing both C and L bands, here we report the successful transmission of 320×114 -Gb/s DWDM signals over 580-km of ULL SMF-28 fiber with a record information capacity of 32-Tb/s, without using Raman amplification. here, note that the capacity is calculated by assuming that the transmitted data payload is solely a 100-Gbit/s Ethernet multiplexed analogue components rate signal. However, if we only consider 7% forward error correction (FEC) overhead, as is used in [25], the transmitted capacity should be 33.9-Tb/s. To achieve the aforementioned results, we have employed two new technologies. First, we employ a more noise-tolerant modulation format, polarization-multiplexed and RZ-shaped 8-ary quadrature amplitude modulation (8QAM) to increase the transmission reach, where the 8QAM signal is generated by using commercial modulators with binary electrical driving signal through a novel synthesizing method. To the best of our knowledge, this is the first optical transmission experiment that uses 8QAM modulation format. Second, we employ a new cascaded multimodulus equalization algorithm for blind polarization demultiplexing of PDM-8QAM optical signals [32]. The proposed new algorithm can achieve better SNR performance than the classic constant modulus algorithm (CMA) for PDM-8QAM signal.

The rest of this paper is organized as follows. In Section II, we describe the proposed high-speed 8QAM modulator technology. Section III is devoted to the DSP algorithms employed

Manuscript received May 15, 2009; revised August 03, 2009. First published September 22, 2009; current version published February 01, 2010.

X. Zhou, P. D. Magill, L. Nelson, M. Birk, and G. Zhang are with AT&T Labs-Research, Middletown, NJ 07748 USA (e-mail: zhoux@research.att.com).

J. Yu, M. Huang, Y. Shao, T. Wang, and M. Cvijetic are with NEC Laboratories America, Inc., Princeton, NJ 08540 USA (e-mail: jianjun@nec-labs.com).

S. Ten, H. B. Matthew, and S. K. Mishra are with Corning Incorporated, Corning, NY 14831 USA (e-mail: tens@corning.com).

Color versions of one or more of the figures in this paper are available online at <http://ieeexplore.ieee.org>.

Digital Object Identifier 10.1109/JLT.2009.2032560

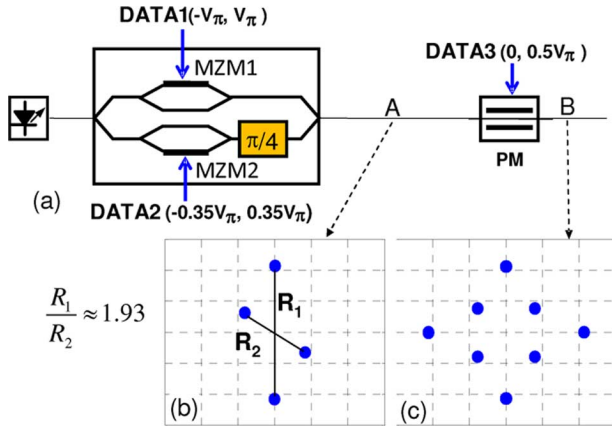


Fig. 1. Schematic illustration of the proposed 8QAM modulator where the constellation diagrams are based on simulation by assuming ideal modulators.

in the coherent receiver, with a special emphasis on the proposed cascaded multimodulus blind equalization algorithm. In Section IV, we describe experimental results employing the modulation and detection techniques described before, including the generation and intradyne detection of 114 Gb/s PDM-RZ-8QAM signal and 32-Tb/s transmission over 580-km of ULL SMF-28 fiber utilizing C + L-band EDFA-only optical amplification. Finally, we present the conclusions in Section V.

II. HIGH-SPEED 8QAM MODULATOR DESIGN

In theory, PDM-8QAM can tolerate 1.5 dB more noise than PDM-8PSK [1], [34] because it encodes the signal in all four dimensions of an optical carrier, and is probably the optimal 64-ary modulation format. Generation of an 8QAM optical signal is not as straightforward as 8PSK because both the phase and the amplitude have to be modulated in a coordinated way. Recently, we experimentally generated 114-Gb/s PDM-8QAM optical signal using a commercial dual-parallel Mach-Zehnder modulator (MZM) followed by a common phase modulator (PM) with binary electrical driving signal through a novel synthesis technique [32]. A different 8QAM generation method has also been reported in [29], where 30-Gb/s 8QAM signal was generated by a special two-state modulator followed by a parallel in-phase/quadrature (I/Q) modulator.

Fig. 1(a) shows a schematic illustration of our method. The proposed 8QAM modulator consists of a $\pi/4$ -biased dual-parallel MZM and a common $(0, \pi/2)$ PM. The two parallel MZMs (MZM1 and MZM2) are both biased at the null point, but use different drive voltages: MZM1 is driven with a full $2 V_\pi$ peak-to-peak signal while MZM2 is only driven with a $0.7 V_\pi$ swing. As a result of this driving condition, the $\pi/4$ -biased dual-parallel MZM introduces both amplitude and phase modulation (of the required amounts) to the original continuous-wave (CW) signal, as shown in Fig. 1(b) by the simulated constellation diagram at the output of the dual-parallel MZM using ideal optical modulators. Then, after $(0, \pi/2)$ phase modulation, an optimal symmetric 8QAM signal is generated, as shown in Fig. 1(c).

The method shown in Fig. 1 allows us to generate 8QAM optical signals using commercially available modulators with binary electrical driving signals. But this 8QAM modulator may

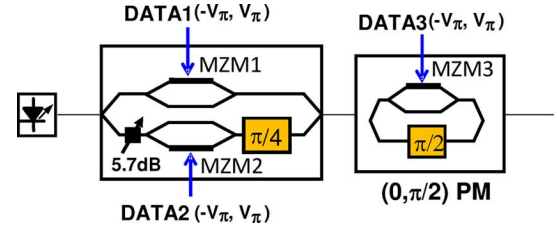


Fig. 2. Modified design of the proposed 8QAM modulator.

have two potential problems when used in a real system. First, the MZM2 inside the dual-parallel MZM is only driven with $0.7 V_\pi$, and therefore, is less tolerant to the transmitter-side band-limiting effects (limited electrical driver amplifier bandwidth and optical modulator electro/optic (E/O) response bandwidth) than the usual case with full $2 V_\pi$ drive. This is due to the fact that the MZM has a nonlinear E/O response function given by $\sin(0.5 \pi V/V_\pi)$ when biased at the null point, where V denotes the driving electrical voltage. Second, the common PM will linearly transfer the amplitude jitter of the driving electrical signal into phase jitter of the generated optical signal, making it very sensitive to the transmitter-side band-limiting effects.

The two issues described before can be solved by a modification in the design, as shown in Fig. 2. In the modified design, the required amplitude modulation imbalance between the upper and the lower branches in the dual-parallel MZM is achieved by introducing an extra 5.7 dB power attenuation in the lower branch (or the higher branch). Note that this power attenuation can also be introduced simply by using an unequal power splitting ratio in the two power couplers located inside the dual-parallel MZM. Such a design allows us to drive both MZM1 and MZM2 with full $2 V_\pi$ peak-to-peak swing. In the modified 8QAM modulator, we also introduce a new MZM-based $(0, \pi/2)$ PM, where the $(0, \pi/2)$ phase modulation is achieved by interfering one $(0, \pi)$ MZM-modulated light with a $\pi/2$ phase-shifted CW light.

In Fig. 3, we show a simulated result of the impact of transmitter bandwidth (normalized to the symbol rate) on the quality of the generated 8QAM optical signal in terms of the maximum constellation deviation (normalized to ideal decision threshold) for the two 8QAM modulator designs. Here, the transmitter consists of all the required optical modulators and their electrical driving circuits. In addition, we have assumed that all the modulators (and their driving electrical circuits) have identical frequency response function. For simplicity, we use a first-order Gaussian filter to emulate the accumulated band-limiting effects in the transmitter: we first generate ideal nonreturn-to-zero (NRZ) modulated binary electrical signals with decorrelated $2^9 - 1$ pseudorandom binary sequence (PRBS) data pattern; next, we pass these binary electrical signals through a first-order Gaussian filter to emulate transmitter-side band-limiting effects; and finally, we use the filtered electrical binary signals to drive ideal optical modulators. As expected, it can be seen that the modified design shown in Fig. 2 requires significantly lower transmitter bandwidth than the original design shown in Fig. 1.

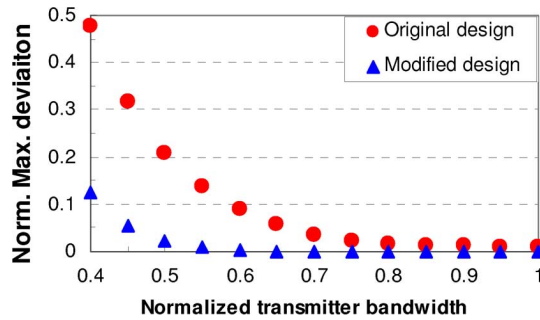


Fig. 3. Simulated maximum constellation deviation versus normalized 3-dB transmitter bandwidth for the two different 8QAM modulator designs.

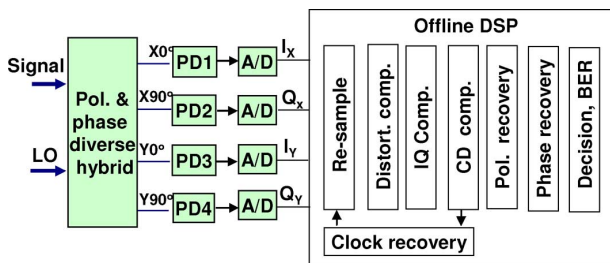


Fig. 4. Illustration of the digital coherent receiver used in the experiments (at stable operation stage).

III. DSP ALGORITHMS

A. Overview of the DSP Algorithms

Fig. 4 shows a schematic illustration of the digital coherent receiver used in our experiments. The incoming optical field is coherently mixed with a local oscillator (LO) through a polarization- and phase-diverse coherent mixer. At the output of this coherent mixer, we have the I/Q components of the received optical field in both X- and Y-polarizations, detected by using four single-ended photodetectors. The detected analog electrical signals are digitized by four analog-to-digital converters (ADCs) and then processed by using offline DSP algorithms through a desktop computer.

At the initial stage of processing (not shown in Fig. 4), we use a free-running clock to resample the digitized signal to a sample rate (approximately) equal to $2 \times$ baud rate, and then we perform digital fiber chromatic dispersion (CD) compensation. After the CD compensation, we extract the clock from the CD-compensated signal using the classic “square and filtering” methods. Once the clock is extracted, we enter into the formal processing stage (see Fig. 4), where the extracted clock (from the previous data block) is used to do the resampling of the following data block. The reason why we require such an initial start stage is because it is very difficult to extract the clock directly from the original CD-uncompensated signal. The free-running clock is digitally generated based on the known knowledge about the clock frequency (but the clock phase is unknown).

The formal DSP stages consist of eight steps. First, we do the resampling, as described in the before. Second, we mitigate the distortion caused by single-ended photodetection due to direct square-law detection of the signal component through a recently proposed DSP algorithm [27]. After this, the quadrature imbalance caused by the imperfect coherent mixer is compensated by

using the Gram–Schmidt orthogonalization procedure (GSOP) [35], [36]. The GSOP enables a set of nonorthogonal samples to be transformed into a set of orthogonal samples. Assuming that the two received signals, r_I and r_Q , are nonorthogonal through GSOP, we can obtain a new pair of orthonormal signals, denoted by r'_I and r'_Q , as follows:

$$r'_I(t) = \frac{r_I(t)}{\sqrt{P_I}} \quad (1)$$

$$r'_Q(t) = \frac{(r_Q(t) - \rho \frac{r_I(t)}{\sqrt{P_I}})}{\sqrt{P_Q}} \quad (2)$$

where $\rho = \langle r_I(t) \cdot r_Q(t) \rangle$ is the correlation coefficient, $P_I = \langle r_I^2(t) \rangle$ and $P_Q = \langle r_Q^2(t) \rangle$, and $\langle \cdot \rangle$ denotes the ensemble average operator.

After compensation of I/Q imbalance, we perform digital CD compensation through a fixed T/2-spaced finite impulse response (FIR) filter. The required filter coefficients are obtained from the (approximately) known fiber CD transfer function using a frequency-domain truncation method [18]. To reduce the complexity of CD compensation, fast Fourier transform (FFT) based frequency-domain equalization (FDE) may be used in the real system: unlike the time-domain FIR filter whose computation complexity scales with N^2 (N is the filter length decided by fiber dispersion and baud rate), the computation complexity of FDE only scales with $N \log_2^N$. As described before, clock recovery is carried out following the CD compensation.

In the next step, we perform simultaneous polarization recovery and polarization mode dispersion (PMD)/residual CD compensation with four complex-valued, 13-tap, T/2-spaced adaptive FIR filters, optimized by a new cascaded multimodulus algorithm (CMMA) [32]. Other linear distortions such as optical filtering effects can also be compensated or mitigated by this adaptive equalization. The reason we developed a CMMA for PDM-8QAM signals is because we have found that the classic CMA does not perform well for PDM-8QAM in terms of SNR performance. A detailed description of the proposed new algorithm will be presented in the following section. To increase the convergence speed and robustness of blind polarization recovery, we have used the first-order CMA at the initial equalization stage for pre-convergence. As can be seen in the following section, the first-order CMA is compatible with the proposed CMMA and the extra implementation complexity introduced by adding such a pre-equalization stage is negligible.

Carrier frequency and phase recoveries are performed after polarization demultiplexing. We first use a feedforward M th-power algorithm to estimate the frequency offset between the LO and the received signal source [39], [40], and then use a maximum-likelihood (ML) algorithm [41] with the known 8QAM constellation to estimate the carrier phase. For the M th-power-based frequency recovery, we first normalize the signal and then raise the normalized signal to the 8th-power to remove the data modulation. The frequency offset between the transmitted signal and the LO is decided from the speed of the phase rotation of the resulting signal. ML phase estimation is based on the assumption that the laser phase ψ does not change over multiple symbol periods. Over this period of time,

the ML estimate of ψ is the value that maximizes $P(r|\psi)$, the probability density function (PDF) of the received signal r conditioned on ψ . Assuming white and zero-mean Gaussian noise, the ML estimate of ψ can be expressed as [41]

$$\hat{\psi}_{\text{ML}} = -\tan \left[\frac{\text{Im} \left(\sum_{n=0}^{K-1} I_n^* r_n \right)}{\text{Re} \left(\sum_{n=0}^{K-1} I_n^* r_n \right)} \right] \quad (3)$$

where K denotes the number of symbols over which ψ does not change and I is the correctly detected signal which is estimated through an iterative method (the phase of the start block is estimated by using a blind phase search method).

After carrier recovery, we finally make the decision, and perform differential decoding, Gray-code mapping, and BER counting. Note that differential decoding will result in increased bit error rate (BER) (as compared to the case using absolute phase synchronization through training sequence) because one original symbol error may result in two adjacent symbol errors after decoding. But differential decoding can effectively solve the phase ambiguity problem without using a training sequence.

B. Cascaded Multimodulus Algorithm

The classic CMA has been shown to be very effective for blind polarization demultiplexing of PDM-QPSK and PDM-8PSK signals. It has been shown that CMA-based blind equalization can achieve a performance close to decision-directed least-mean-square (DD-LMS) algorithm [18], and therefore can be used as a stand-alone polarization demultiplexing algorithm. As compared to the DD-LMS, the CMA is a decision-independent algorithm. It allows us to perform polarization demultiplexing and carrier phase recovery within different functional blocks, which cannot be realized by using a decision-dependent algorithm such as the DD-LMS. In addition, the performance of DD-LMS depends on the operating error rate and may fail with long error bursts.

However, for PDM-8QAM, we have found that the classic CMA becomes much less effective (in terms of SNR performance) and can no longer be used as a stand-alone equalization algorithm. This is because an 8QAM signal does not present constant symbol amplitude. As a result, the CMA error signal will not approach zero even for an ideal 8QAM signal, resulting in extra noise after equalization. To address this problem, here we describe a new equalization algorithm for decision-independent, blind polarization recovery. The principle of the proposed new algorithm in terms of the error signal calculation method for PDM-8QAM is illustrated in Fig. 5, where we show an ideal circular 8-QAM signal, the equation for error signal calculation, and the calculated intermediate and final errors. For this algorithm, two reference circles with modulus of $(R_1 + R_2)/2$ and $(R_1 - R_2)/2$ are introduced in a cascaded way, such that the final error signal will approach zero for an ideal 8QAM signal. Note that R_1 and R_2 denote the radius of the two circles where the 8QAM constellation points are located. For comparison, the error signal for the classic CMA is calculated using only one reference circle with a constant modulus of $E|Z|^2/E|Z|$ [38]. It is clear that for PDM-8QAM, the CMA cannot have zero error even after perfect equalization.

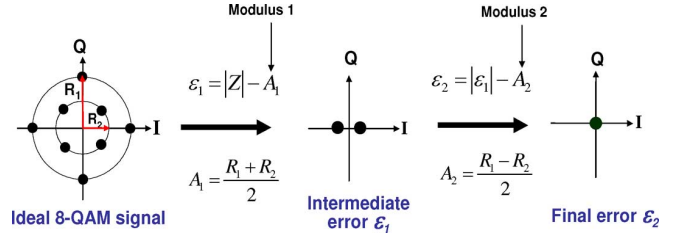


Fig. 5. Illustration of the proposed algorithm for PDM-8QAM signals.

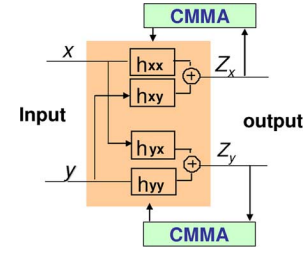


Fig. 6. 2×2 adaptive equalizer used in the coherent receiver, where each h_{ij} is an FIR filter with tap coefficients updated by using the new CMMA.

For the proposed new algorithm, the filter tap weight updated equations for each of the four FIR filters in the 2×2 adaptive equalizer (see Fig. 6) can be obtained by using the classic stochastic gradient algorithm [41], [18]. Given $x(n)$ and $y(n)$ as the two inputs of the adaptive equalizer, the two outputs, $Z_x(n)$ and $Z_y(n)$, can be represented as follows:

$$\begin{aligned} Z_x(n) &= \sum_{k=0}^{K-1} h_{xx}(n, k)x(n-k) \\ &\quad + \sum_{k=0}^{K-1} h_{xy}(n, k)y(n-k) \\ &= \mathbf{h}_{xx}^T \cdot \mathbf{x} + \mathbf{h}_{xy}^T \cdot \mathbf{y} \end{aligned} \quad (4)$$

$$\begin{aligned} Z_y(n) &= \sum_{k=0}^{K-1} h_{yy}(n, k)y(n-k) \\ &\quad + \sum_{k=0}^{K-1} h_{yx}(n, k)x(n-k) \\ &= \mathbf{h}_{yy}^T \cdot \mathbf{y} + \mathbf{h}_{yx}^T \cdot \mathbf{x} \end{aligned} \quad (5)$$

where h_{xx} , h_{xy} , h_{yy} , and h_{yx} are adaptive FIR filters, each of which have length K taps. Based on the new algorithm, the two error signals ε_x and ε_y are given by

$$\varepsilon_x = ||Z_x| - A_1| - A_2 \quad (6)$$

$$\varepsilon_y = ||Z_y| - A_1| - A_2 \quad (7)$$

where A_1 and A_2 denote the two moduli used for error signal calculation (see Fig. 5). For an amplitude-normalized signal, we should have $A_1 = 1$ and $A_2 = 0.32$. Typically, the equalizer will attempt to minimize the mean square error, which gives the following criteria:

$$\frac{d\langle \varepsilon_x^2 \rangle}{d\mathbf{h}_{xx}} = 0 \quad \frac{d\langle \varepsilon_x^2 \rangle}{d\mathbf{h}_{xy}} = 0 \quad \frac{d\langle \varepsilon_y^2 \rangle}{d\mathbf{h}_{yy}} = 0 \quad \frac{d\langle \varepsilon_y^2 \rangle}{d\mathbf{h}_{yx}} = 0. \quad (8)$$

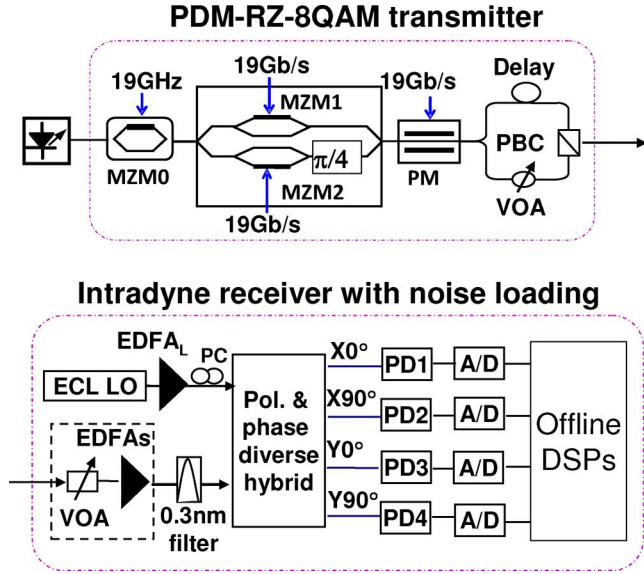


Fig. 7. Experimental setup for the generation and intradyne detection of RZ-shaped 114-Gb/s PDM-8QAM signal.

To find the optimal tap weights, we replace the gradients by their instantaneous values, and then, we will have the following tap weight updating equations:

$$\mathbf{h}_{xx} \rightarrow \mathbf{h}_{xx} + \mu \varepsilon_x e_x \cdot \bar{\mathbf{x}} \quad (9)$$

$$\mathbf{h}_{xy} \rightarrow \mathbf{h}_{xy} + \mu \varepsilon_x e_x \cdot \bar{\mathbf{y}} \quad (10)$$

$$\mathbf{h}_{yx} \rightarrow \mathbf{h}_{yx} + \mu \varepsilon_y e_y \cdot \bar{\mathbf{x}} \quad (11)$$

$$\mathbf{h}_{yy} \rightarrow \mathbf{h}_{yy} + \mu \varepsilon_y e_y \cdot \bar{\mathbf{y}} \quad (12)$$

where

$$e_{x,y} = \text{sign}(|Z_{x,y}| - A_1) \cdot \text{sign}(Z_{x,y}). \quad (13)$$

In the previous equations, $\text{sign}(x)$ is a sign function given by $x/|x|$, μ is a convergence parameter, and $\bar{\mathbf{x}}$ and $\bar{\mathbf{y}}$ denote the complex conjugates of \mathbf{x} and \mathbf{y} , respectively.

We have observed that the proposed new algorithm can achieve significantly better SNR performance than the classic CMA; however, its convergence performance is slightly worse. To improve both SNR and convergence performance, we can use the classic CMA in the initial equalization stage for pre-convergence and then switch to the proposed CMMA for formal equalization to achieve the (approximately) optimal SNR performance. Note that the proposed CMMA is backward compatible to the classic CMA: simply by setting $A_1 = 0$ and $A_2 = 1$, the proposed CMMA becomes the classic first-order CMA. So, adding a first-order CMA-based initial equalization at the start stage introduces negligible implementation complexity.

IV. EXPERIMENTS

A. Generation and Detection of 114-Gb/s PDM-RZ-8QAM

The experimental setup for generation and intradyne detection of RZ-shaped 114-Gb/s PDM-8QAM signal with optical

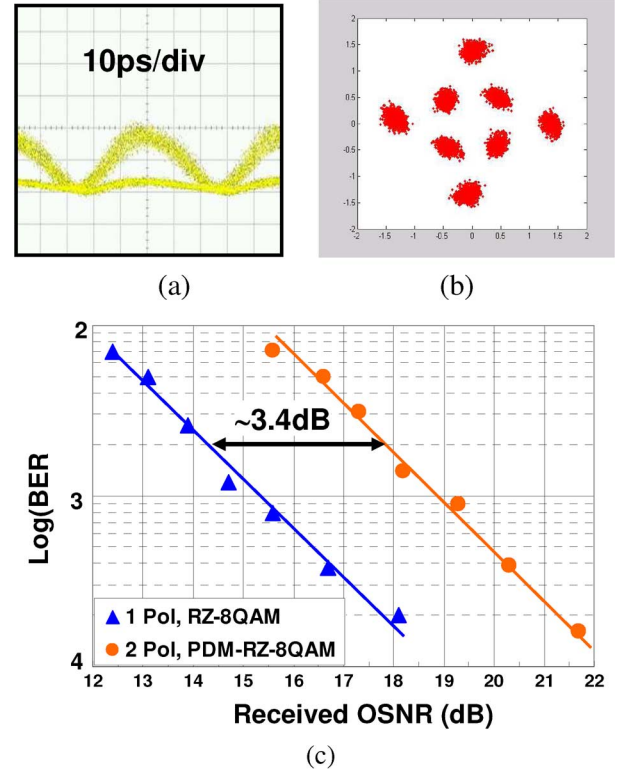


Fig. 8. Measured single-channel back-to-back performance. (a) Eye diagram through direct detection, (b) recovered constellation diagram without adding noise, and (c) BER versus received OSNR for single-polarization 57 Gb/s RZ-8QAM and 114 Gb/s PDM-RZ-8QAM.

noise loading is shown in Fig. 7. The 8QAM modulator consists of a $\pi/4$ -biased commercial dual-parallel MZM with a 3 dB bandwidth of about 19 GHz and a common $(0, \pi/2)$ PM with a 3 dB bandwidth greater than 25 GHz. The 8QAM modulator was driven by three 19-Gb/s binary electrical signals, each generated by time-division-multiplexing four 4.75-Gb/s $2^{11} - 1$ PRBS signals. To introduce $\sim 50\%$ RZ-pulse shaping, a common MZM (i.e., MZM0) is added before the dual-parallel MZM, driven by a 19 GHz sinusoidal clock. The generated 8QAM signal is then divided and recombined with about 1.6 ns time delay by using a polarization beam combiner (PBC) to generate the required PDM-8QAM signal. At the receiver, amplified spontaneous emission (ASE) noise is added by attenuating the signal before an optical amplifier. The amplified signal passes through a 0.3 nm optical filter, and then is mixed with the LO signal in a polarization and phase-diverse hybrid. Note that we use a narrow linewidth (~ 100 kHz) external cavity laser (ECL) for both the LO and the signal source. The frequency of the LO is tuned to within 200-MHz of the transmit laser. At the output of the optical hybrid, four single-ended photodetectors are used to convert the optical signals into electrical signals. The sampling and digitization (A/D) function is achieved with a four-channel real-time sampling scope (50 GSa/s, 16-GHz electrical bandwidth, and 5.5 bit effective resolution). The captured data are then postprocessed in a desktop computer using the algorithms described in the previous section.

In Fig. 8(a)–(c), we show the measured single-channel back-to-back performance for the generated 114-Gb/s

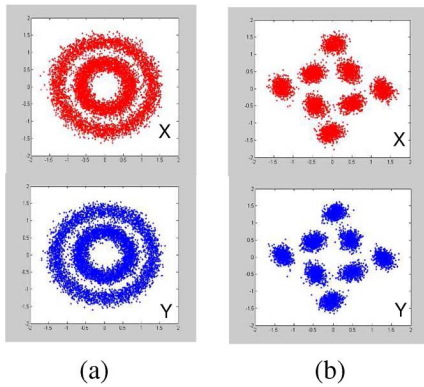


Fig. 9. Recovered constellation diagrams of both X- and Y-polarizations using the proposed new equalization algorithm with OSNR = 18.5 dB, where (a) shows the result after polarization recovery, while (b) is after carrier recovery.

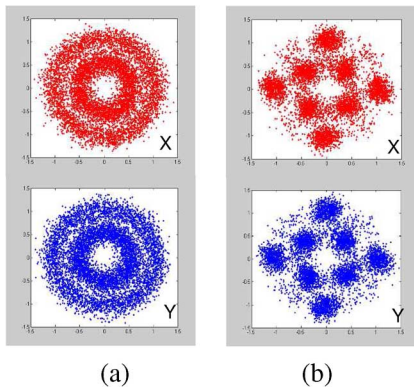


Fig. 10. Recovered constellation diagrams of both X- and Y-polarizations using the classic CMA with OSNR = 18.5 dB, where (a) shows the result after polarization recovery, while (b) is after carrier recovery.

PDM-RZ-8QAM signal. Fig. 8(a) shows the electrical eye diagram through direct square-law detection, Fig. 8(b) shows the recovered constellation diagram without adding ASE noise loading, and Fig. 8(c) shows the BER versus received optical SNR (OSNR) for both 57-Gb/s single-polarization RZ-8QAM and 114-Gb/s PDM-RZ-8QAM signals. Note that throughout this paper, the BER is calculated based on 2.6×10^6 bits. To achieve a BER 2×10^{-3} , the required OSNR is 17.8 dB for the generated 114-Gb/s PDM-RZ-8QAM signal, which is more than 1 dB better than our previously reported results using PDM-RZ-8PSK modulation format [22], but is still more than 2.5 dB away from our simulated results [34]. Among the 2.5 dB OSNR penalty, 0.4 dB comes from the excessive PDM penalty (may be due to imperfect polarization demultiplexing), as is shown in Fig. 8(c).

By using the proposed new CMMA, the recovered constellation diagrams after polarization and phase recovery with OSNR = 18.5 dB are shown in Fig. 9(a) and (b), respectively. As a comparison, the corresponding results using the classic CMA are shown in Fig. 10(a) and (b). Note that the convergence parameters have been optimized for both cases. One can observe the improvement in the quality of the recovered signals due to the proposed CMMA as compared to the classic CMA.

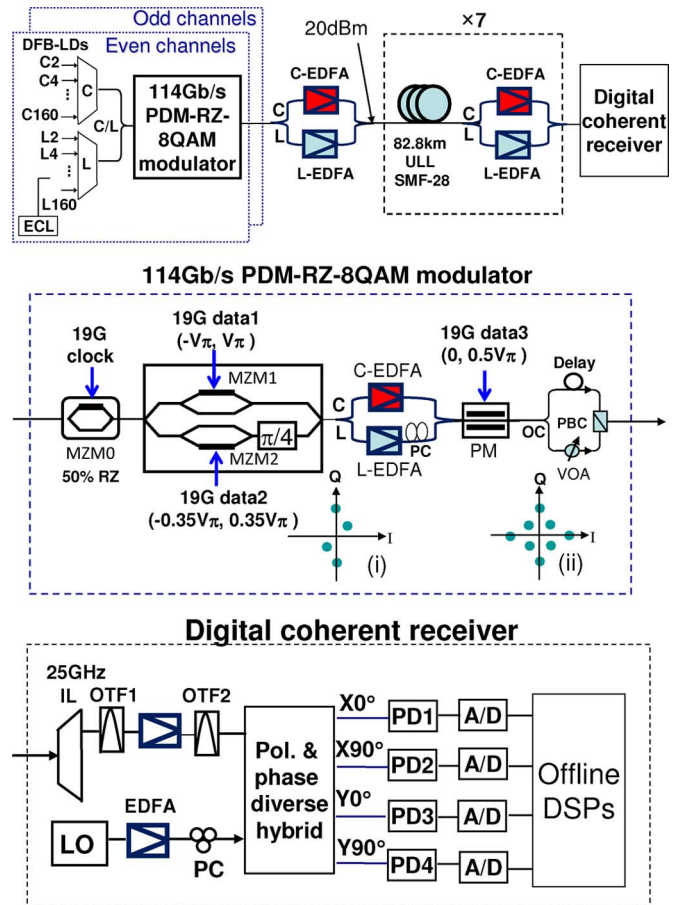


Fig. 11. Experimental setup for 32 Tb/s C + L-band transmission experiment. IL: interleaver, PC: polarization controller, OTF: optical tunable filter, and PD: photodetector.

B. 32 Tb/s C + L-Band Transmission Over 580 km ULL SMF-28

The experimental setup for 32 Tb/s PDM-RZ-8QAM transmission is shown in Fig. 11. The details of the 114-Gb/s PDM-RZ-8QAM modulator are described in the previous section. Here, note that we have added a C + L-band EDFA between the dual-parallel MZM and the $(0, \pi/2)$ PM. For this DWDM experiment, we built two transmitters: one for the 160 C + L-band odd wavelength channels and the other for the 160 C + L-band even channels. The 50 GHz spaced odd and the even channels are combined through a flat-top interleaver (14-GHz bandwidth at 0.5 dB and 34-GHz at 20 dB). The two sets of 50 GHz-spaced wavelengths were obtained by the use of eight 40×1 WDM multiplexer (with 100 GHz spacing) and four 3-dB couplers (all are polarization-maintained optical components). The sources of the 320 channels are all from conventional DFB lasers (linewidth ~ 5 MHz). Since the phase noise of DFB lasers is too large for 8QAM modulation, an extra C + L-band tunable ECL with linewidth ~ 100 kHz is introduced for BER measurement: the selected channel is switched from the DFB source to a tunable ECL source during each measurement. In the two transmitters, we use polarization-maintaining C/L combiners, optical couplers, and C-band EDFAs; the L-band EDFAs are not polarization maintaining (due to availability), requiring polarization controllers (PCs)

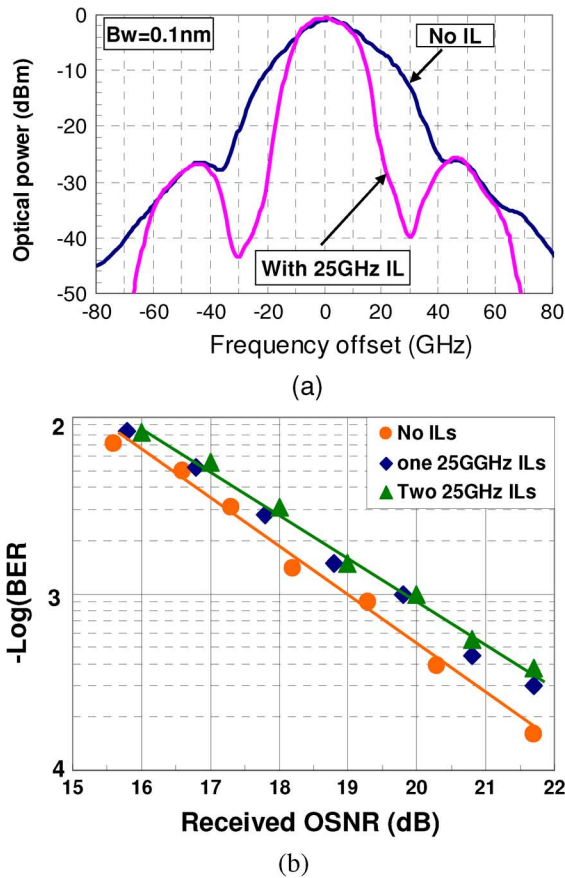


Fig. 12. Impact of narrow optical filtering on the generated 114-Gb/s PDM-RZ-8QAM signal, where (a) shows the optical spectra and (b) gives the measured BER versus OSNR with and without the 25 GHz interleavers.

before the PMs. These PCs are found to be stable, requiring adjustment in the time scale of about 1 h.

The line system consists of seven spans of ITU-T G.652 compliant Corning SMF-28 ULL fiber (82.8 km average length) and EDFA-only optical amplification. At 1550 nm, the measured average fiber loss is 0.169 dB/km (14.6 dB/span with connector loss included) and the average dispersion is 15.9 ps/nm (17.6 ps/nm-km at 1580 nm). In this experiment, we used no optical dispersion compensation. Gain-flattened two-stage EDFAs are used to compensate for the span loss. The total launch power into the transmission fiber is 20 dBm (17 dBm for both the C-band and L-band), corresponding to -5 dBm per channel. At such a launch power, stimulated Raman scattering introduces 2.5 dB/span gain tilt across the C + L bandwidth. This Raman tilt is compensated every span by introducing an opposite EDFA tilt through a midstage variable attenuator. For the 580 km transmission link, the measured total link PMD is 0.485 ps.

At the receiver, the measured channel is selected following a 25 GHz deinterleaver with two optical tunable filters, OTF1 (0.3 nm for the C-band and 0.55 nm for the L-band) and OTF2 (1 nm for both the C- and L-bands). We use a full C + L-band tunable ECL with ~ 100 -kHz linewidth as the LO. As described in the previous section, four single-ended photodetectors followed by a four-channel real-time sampling scope are used to convert optical signal into digitized electrical signal.

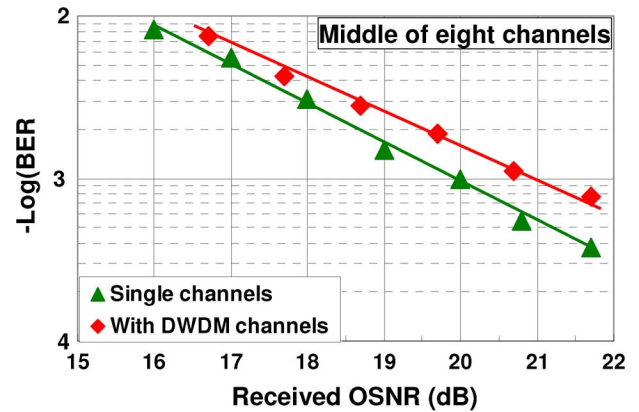


Fig. 13. Measured results on the impact of DWDM crosstalk for 25 GHz channel spacing.

Experimental results are presented in Figs. 12-15. In Fig. 12(a) and (b), we show the impact of 25 GHz interleaver on the generated 114-Gb/s PDM-RZ-8QAM signal in a back-to-back measurement. One can see that two cascaded 25-GHz interleavers only result to about 0.6 dB OSNR penalty at BER 2×10^{-3} . The measured results on the impact of DWDM crosstalk are shown in Fig. 13, where the BER of the middle channel (total of eight channels for this measurement) versus received OSNR with and without neighboring DWDM channels are displayed. One can see that the DWDM crosstalk introduces about 0.9 dB OSNR penalty at 2×10^{-3} .

The results for the 32 Tb/s transmission experiment are shown in Figs. 14 and 15. In Fig. 14(a)–(c), we show the measured optical spectra of the 160 odd-channel signal without modulation, and the modulated 320-channel signal before and after transmission, respectively. The transmitted OSNRs in a 0.1 nm noise bandwidth at 1532.4 (the shortest wavelength), 1564.07, 1569.94, and 1603.3 nm (the longest wavelength) are 29.9, 34, 31, and 30.5 dB, respectively. After 580 km transmission, the OSNR decreases to 22.1, 24.8, 24.1, and 23.6 dB, accordingly. The measured BERs (an average of both X- and Y-polarization) for all the 320 channels are shown in Fig. 15, where the inset shows the received constellation diagrams at 1539.97 nm, which is among the worst performing channels. As shown in Fig. 18, all 320 channels have a BER below the enhanced FEC threshold 2×10^{-3} . Note that the BER spectrum (BER versus wavelength) shown in Fig. 15 is different from the received OSNR spectrum shown in Fig. 14(c). The reason may lie in the following two factors. 1) The BER performance of each wavelength channel depends not only on the received OSNR, but also on the impact of fiber nonlinear effects: the channel with higher receiving OSNR usually suffers more from the fiber nonlinear effects and therefore not necessarily results to a better BER performance. 2) The back-to-back performance difference between different channels may not be trivial due to the use of multiple cascaded optical modulators in the transmitter. We did not use any channel power emphasis at the transmitter side [see Fig. 14(b)], but tilt preemphasis has been introduced in some of the inline optical amplifiers (in span 2, 4, and 6) to improve the OSNR performance of the shorter wavelength channel.

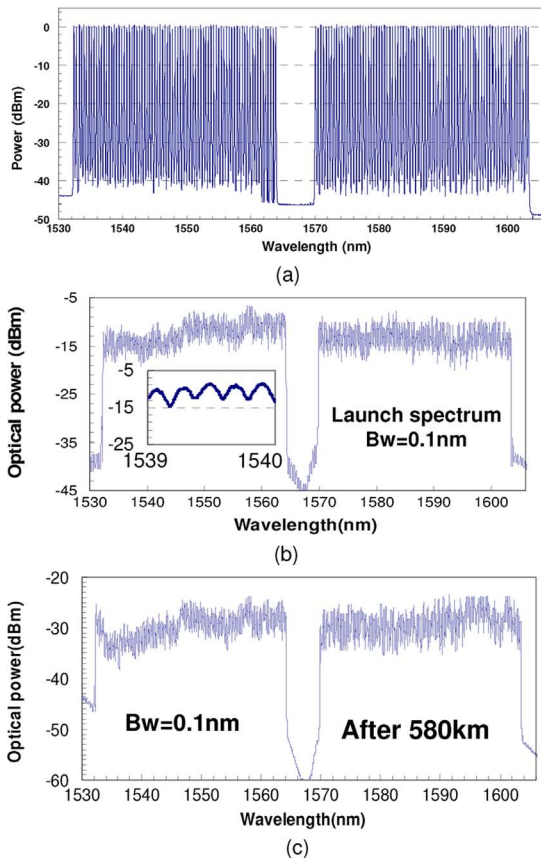


Fig. 14. Monitored optical spectra (in 0.1 nm resolution) of: (a) 160 odd channels before modulation, (b) 320 channels before transmission, and (c) 320 channels after 580 km transmission.

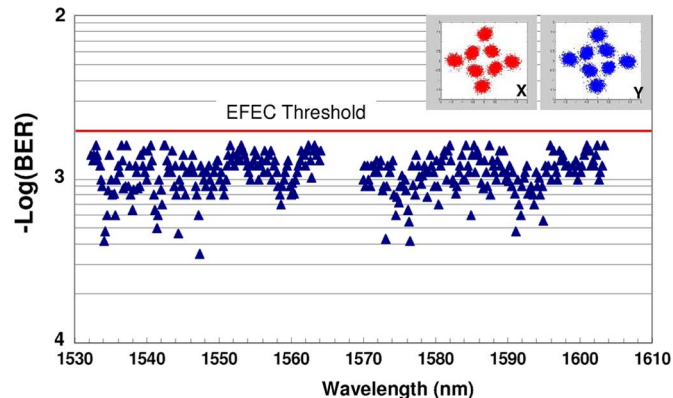


Fig. 15. Measured BERs for 320 channels after 580 km transmission. (Inset) Received constellation diagram at 1539.97 nm.

V. CONCLUSION

We have proposed a novel synthesizing method for high-speed 8QAM optical signal generation, employing only commercial optical modulators with binary electrical drive signals. With the proposed method, we successfully generated a 114 Gb/s PDM-8QAM optical signal using a commercial dual-parallel MZM followed by a common $(0, \pi/2)$ PM. Through simulation, we also show that the performance of the proposed high-speed 8QAM modulator can be improved

by a modification in the design of dual-parallel MZM and by introducing an MZM-based $(0, \pi/2)$ PM.

To improve the reception of the generated PDM-8QAM optical signal through intradyne detection, a new cascaded multimodulus equalization algorithm has been proposed for blind polarization demultiplexing of PDM-8QAM signal. We experimentally show that the proposed algorithm can achieve significantly better signal-to-noise performance than the classic CMA.

Using the proposed high-speed 8QAM modulator technology and blind equalization algorithm, we have demonstrated successful transmission of a record 32-Tb/s fiber capacity (320×114 Gb/s) over 580 km of ULL SMF-28 fiber utilizing C + L-band EDFA-only optical amplification and single-ended coherent detection technique, at a spectral efficiency of 4.0 bit/s/Hz.

ACKNOWLEDGMENT

The authors would like to thank Y. Yano and his colleagues from OND NEC Japan, D. Qian, P. N. Ji, and L. Xu from NEC Labs, and K. C. Reichmann and P. P. Iannone from AT&T Labs-Research for their support in this experiment.

REFERENCES

- [1] J. M. Kahn and K. P. Ho, "Spectral efficiency limits and modulation/detection techniques for DWDM systems," *IEEE J. Sel. Topics Quantum Electron.*, vol. 10, no. 2, pp. 259–272, Mar./Apr. 2004.
- [2] A. H. Gnauck and P. J. Winzer, "Optical phase-shift-keyed transmission," *J. Lightw. Technol.*, vol. 23, no. 1, pp. 115–130, Jan. 2005.
- [3] S. Tsukamoto, D. S. Ly-Gagnon, K. Katoh, and K. Kikuchi, "Coherent demodulation of 40-Gbit/s polarization-multiplexed QPSK signals with 16-GHz spacing after 200-km transmission," in *Proc. OFC 2005*, Anaheim, CA, p. 3, Paper PDP-29.
- [4] P. J. Winzer, G. Raybon, S. Chandrasekhar, C. D. Doerr, T. Kawashishi, T. Sakamoto, and K. Higuma, "10 × 107 Gb/s NRZ-DQPSK transmission at 1.0 b/s/Hz over 12 × 100 km including 6 optical routing nodes," in *Proc. OFC 2007*, Anaheim, CA, p. 3, Paper PDP 24.
- [5] A. H. Gnauck, G. Charlet, P. Tran, P. J. Winzer, C. Doerr, J. Centanni, E. Burrows, T. Kawashishi, T. Sakamoto, and K. Higuma, "25.6-Tb/s C + L-band Transmission of polarization-multiplexed RZ-DQPSK signals," presented at the OFC 2007, Anaheim, CA, Mar., Paper PDP-19.
- [6] S. Chandrasekhar, X. Liu, E. C. Burrows, and L. L. Buhl, "Hybrid 107 Gb/s polarization-multiplexed DQPSK and 42.7-Gb/s DQPSK transmission at 1.4-bits/Hz spectral efficiency over 1280 km of SSMF and 4 bandwidth-managed ROADMs," presented at the ECOC 2007, Berlin, Germany, Sep., Paper PD 1.9.
- [7] Y. Han and G. Li, "Coherent optical communication using polarization multiple-input-multiple-output," *Opt. Exp.*, vol. 13, pp. 7527–7534, 2005.
- [8] S. L. Jansen, R. H. Derksen, C. Schubert, X. Zhou, M. Birk, C.-J. Weiske, M. Bohn, D. van den Borne, P. M. Krummrich, M. Möller, F. Horst, B. J. Offrein, H. de Waardt, G. D. Khoe, and A. Kirstädter, "107-Gb/s full-ETDM transmission over field installed fiber using vestigial sideband modulation," presented at the OFC 2007, Anaheim, CA, Paper OWE3.
- [9] H. Masuda, A. Sano, T. Kobayashi, E. Yoshida, Y. Miyamoto, Y. Hibino, K. Hagimoto, T. Yamada, T. Furuta, and H. Fukuyama, "20.4 Tb/s (204×111 Gb/s) transmission over 240 km using bandwidth-maximized hybrid Raman/EDFAs," presented at the OFC 2007, Anaheim, CA, Paper PDP20.
- [10] C. R. S. Fludger, T. Duthel, D. Van den Borne, C. Schülten, E. D. Schmidt, T. Wuth, E. De Man, G. D. Khoe, and H. de Waardt, "10 × 111 Gb/s, 50 GHz spaced, POLMUX-RZ-DQPSK transmission over 2375 employing coherent equalization," presented at the OFC 2007, Anaheim, CA, Paper PDP 22.
- [11] M. Nakazawa, J. Hongo, K. Kasai, and M. Yoshida, "Polarization-multiplexed 1 Gsymbol/s 64QAM (12 Gb/s) coherent optical transmission over 150 km with an optical bandwidth of 2 GHz," presented at the OFC 2007, Anaheim, CA, Paper PDP26.

- [12] X. Zhou, J. Yu, M. Du, and G. Zhang, "2 Tb/s (20×107 Gb/s) RZ-DQPSK straight-line transmission over 1005 km of standard single mode fiber (SSMF) without Raman amplification," presented at the OFC 2008, San Diego, CA, Paper OMQ3.
- [13] S. L. Jansen, I. Morita, and H. Tanaka, "10 \times 121.9-Gb/s PDM-OFDM transmission with 2-b/s/Hz spectral efficiency over 1000 km of SSMF," presented at the OFC 2008, San Diego, CA, Paper PDP2.
- [14] H. Sun, K.-T. Wu, and K. Roberts, "Real-time measurements of a 40 Gb/s coherent system," *Optics Exp.*, vol. 16, no. 2, pp. 873–879, 2008.
- [15] L. E. Nelson, S. L. Woodward, S. Foo, X. Zhou, M. D. Feuer, D. Hanson, D. McGhan, H. Sun, M. Moyer, M. O. Sullivan, and P. D. Magill, "Performance of a 46-Gb/s dual-polarization QPSK transceiver in a high-PMD fiber transmission experiment," presented at the OFC 2008, San Diego, CA, Mar., Paper PDP-19.
- [16] N. Kikuchi, K. Mandai, K. Sekine, and S. Sasaki, "Incoherent 32-level optical multilevel, signaling technologies," *J. Lightw. Technol.*, vol. 26, no. 1, pp. 150–157, Jan. 2008.
- [17] M. G. Taylor, "Coherent detection method using DSP for demodulation of signal and subsequent equalization of propagation impairments," *IEEE Photon. Technol. Lett.*, vol. 16, no. 2, pp. 674–676, Feb. 2004.
- [18] S. J. Savory, "Digital filters for coherent optical receivers," *Optics Exp.*, vol. 16, no. 2, pp. 804–817, 2008.
- [19] G. Charlet, J. Renaudier, H. Mardoyan, P. Tran, O. B. Pardo, F. Verluise, M. Achouche, A. Boutin, F. Blache, J. Dupuy, and S. Bigo, "Transmission of 16.4 Tbit/s capacity over 2550 km using PDM QPSK modulation format and coherent receiver," presented at the OFC 2008, San Diego, CA, 2008, Paper PDP3.
- [20] M. Seimetz, L. Molle, D.-D. Gross, B. Auth, and R. Freund, "Coherent RZ-8PSK transmission at 30 Gb/s over 1200 km employing Homodyne detection with digital carrier phase estimation," presented at the ECOC 2007, Berlin, Germany, Sep., Paper We.8.3.4.
- [21] Y. Ma and W. Shieh, "107 Gb/s coherent optical OFDM reception using orthogonal band multiplexing," in *Proc. OFC 2008*, p. 3, Paper PDP7.
- [22] X. Zhou, J. Yu, D. Qian, T. Wang, G. Zhang, and P. Magill, "8 \times 114 Gb/s, 25-GHz-spaced, polmux-RZ-8PSK transmission over 640 km of SSMF employing digital coherent detection and EDFA-only amplification," presented at the OFC 2008, San Diego, CA, Mar., Paper PDP1.
- [23] P. J. Winzer and A. H. Gnauck, "112-Gb/s polarization-multiplexed 16-QAM on a 25-GHz WDM grid," in *Proc. ECOC 2008*, Sep., pp. 1–2, Paper Th.3.E.5.
- [24] J. Yu, X. Zhou, D. Qian, M. F. Huang, P. N. Ji, and G. Zhang, "20 \times 112 Gbit/s, 50 GHz spaced, PolMux-RZ-QPSK straight-line transmission over 1540 km of SSMF employing digital coherent detection and pure EDFA amplification," presented at the ECOC 2008, Brussel, Belgium, Sep., Paper Th.2.A.2.
- [25] J. Yu, X. Zhou, M. F. Huang, Y. Shao, D. Qian, T. Wang, M. Cvijetic, P. Magill, L. Nelson, M. Birk, S. Ten, H. B. Matthew, and S. K. Mishra, "17 Tb/s (161×114 Gb/s) PolMux-RZ-8PSK transmission over 662 km of ultra-low loss fiber using C-band EDFA amplification and digital coherent detection," presented at the ECOC 2008, Brussel, Belgium, Sep., Paper PDP Th.3.E.2.
- [26] Y. Mori, C. Zhang, K. Igarashi, K. Katoh, and K. Kikuchi, "Unrepeated 200-km transmission of 40-Gbit/s 16-QAM signals using digital coherent optical receiver," in *Proc. OECC 2008*, pp. 1–2, Paper PDP 4..
- [27] X. Zhou, J. Yu, and D. Qian, "A novel DSP algorithm for improving the performance of digital coherent receiver using single-ended photo detection," presented at the ECOC 2008, Brussel, Belgium, Paper Mo.4.D.1.
- [28] R. Freund, D. D. Grob, M. Seimetz, L. Molle, and C. Caspar, "30 Gbit/s RZ-8-PSK transmission over 2800 km standard single mode fiber without inline dispersion compensation," presented at the OFC 2008, San Diego, CA, Paper OMI5.
- [29] N. Kikuchi, K. Mandai, and S. Sasaki, "Experimental demonstration of incoherent optical multilevel staggered-APSK (amplitude and phase shift keying) signaling," presented at the OFC 2008, San Diego, CA, Mar., Paper OMI3.
- [30] J. Yu, X. Zhou, M. F. Huang, D. Qian, L. Xu, and P. N. Ji, "Transmission of hybrid 112 and 44 Gb/s PolMux-QPSK in 25 GHz channel spacing over 1600 km SSMF employing digital coherent detection and EDFA-only amplification," presented at the OFC 2009, San Diego, CA, Mar., Paper OThR3.
- [31] X. Zhou, J. Yu, D. Qian, T. Wang, G. Zhang, and P. Magill, "High spectral-efficiency 114 Gb/s transmission using PolMux-RZ-8PSK modulation format and single-ended digital coherent detection technique," *J. Lightw. Technol.*, vol. 27, no. 3, pp. 146–152, Feb. 2009.
- [32] X. Zhou, J. Yu, and P. D. Magill, "Cascaded two-modulus algorithm for blind polarization de-multiplexing of 114-Gb/s PDM-8-QAM optical signals," presented at the OFC 2009, San Diego, CA, Mar., Paper OWG3.
- [33] X. Zhou, J. Yu, M. Huang, Y. Shao, T. Wang, P. D. Magill, M. Cvijetic, L. Nelson, M. Birk, G. Zhang, S. Ten, H. B. Matthew, and S. K. Mishra, "32 Tb/s (320×114 Gb/s) PDM-RZ-8QAM transmission over 580 km of SMF-28 ultra-low-loss fiber," presented at the OFC 2009, San Diego, CA, Paper PDPB4.
- [34] X. Zhou and J. Yu, "Multi-level, multi-dimensional coding for high-speed and high spectral-efficiency optical transmission," *J. Lightw. Technol.*, vol. 27, no. 16, pp. 3641–3653, Aug. 2009.
- [35] I. Fatadin, S. J. Savory, and D. Ives, "Compensation of quadrature imbalance in an optical QPSK coherent receiver," *IEEE Photon. Technol. Lett.*, vol. 20, no. 20, pp. 1733–1735, Oct. 2008.
- [36] S. Haykin, *Adaptive Filter Theory*. Englewood Cliffs, NJ: Prentice-Hall, 1986.
- [37] B. Spinnler, "Recent advances on polarization multiplexing," presented at the ECOC 2008, Brussel, Belgium, Sep., Paper TuD2.3..
- [38] D. N. Godard, "Self-recovering equalization and carrier tracking in two-dimensional data communication systems," *IEEE Trans. Commun.*, vol. 28, no. 11, pp. 1867–1875, Nov. 1980.
- [39] A. J. Viterbi and A. M. Viterbi, "Nonlinear estimation of PSK-modulated carrier phase with application to burst digital transmission," *IEEE Trans. Inf. Theory*, vol. IT-29, no. 4, pp. 543–551, Jul. 1983.
- [40] A. Leven, "Frequency estimation in intradyne reception," *IEEE Photon. Technol. Lett.*, vol. 19, no. 6, pp. 366–368, Mar. 2007.
- [41] J. G. Proakis, *Digital Communications*, 4th ed. New York: McGraw-Hill, ch. 6.



Xiang Zhou (M'00–SM'05) received the B.Sc. degree in physics from Fudan University, Shanghai, China, in 1991, and the Ph.D. degree in electrical engineering from Beijing University of Posts and Telecommunications, Beijing, China, in 1999.

From 1999 to 2001, he was with Nangang Technological University, Singapore, as a Research Fellow, where he was involved with research on optical code division multiple access and wideband Raman amplification. Since October 2001, he has been a Senior Member Technical Staff with AT&T Labs-Research, Middletown, NJ, working on optical technologies for ultralong haul optical transmission and photonic networking. He is the author or coauthor of more than 60 papers published in various journals and conference proceedings. He is the holder of 17 USA patents.



Jianjun Yu (M'03–SM'04) received the M.E. and Ph.D. degrees in electrical engineering from Beijing University of Posts and Telecommunications, Beijing, China, in April 1996 and January 1999, respectively.

From June 1999 to January 2001, he was with the Research Center COM, Technical University of Denmark, Lyngby, Denmark, as an Assistant Research Professor. From February 2001 to December 2002, he was with Lucent Technologies and Agere Systems, New Jersey, as a member of the technical staff. In January 2003, he joined Georgia Institute of Technology, Atlanta, where he was a Research Faculty and the Director of the Optical Network Laboratory. He is currently a member of the Senior Member of Technical Staff with the NEC Laboratories America, Princeton, NJ. He is also an Adjunct Professor with Georgia Institute of Technology. He is the author or coauthor of more than 100 papers published in various journals and conference proceedings. He is the holder of three U.S. patents with 15 others pending.

Dr. Yu is an Associate Editor for the IEEE/Optical Society of America (OSA) JOURNAL OF LIGHTWAVE TECHNOLOGY (JLT) and the IEEE/OSA JOURNAL OF OPTICAL COMMUNICATION AND NETWORKING. He was the Guest Editor for a special issue "Convergence of optical and wireless networks" for the IEEE/OSA JLT and "Radio-over-fiber-optical networking" for the *Journal of Optical Networking*. He was a Technical Committee Member (TPC) of the Lasers and Electro-Optics Society 2005–2007 Annual Meeting. He is a TPC of the Optical Fiber Communication Conference and Exposition 2009–2010.



Ming-Fang Huang (S'04) received the B.S. degree in physics from Tamkang University, Taipei, Taiwan, in 2001, and the M.E. and Ph.D. degrees in electro-optical engineering from the National Chiao Tung University, Hsinchu, Taiwan, in 2003 and 2007, respectively.

She is currently a Postdoctoral Fellow in the School of Electrical and Computer Engineering, Georgia Institute of Technology, Atlanta, and also with NEC Laboratories America, Inc., Princeton, NJ. Her research interests include long-haul transmission, new modulation format technologies, high-bit-rate transmission, wavelength-division multiplexing passive optical network, time-division-multiplexing passive optical network, and radio-over-fiber systems.

Yin Shao, photograph and biography not available at the time of publication.

Ting Wang, photograph and biography not available at the time of publication.



Peter Magill received the B.S. degree from the University of Dayton, Dayton, OH, in 1979, and the Ph.D. degree from Massachusetts Institute of Technology, Cambridge, in 1987, both in physics.

In 1987, he joined AT&T Bell Labs, Middletown, NJ, where he was engaged with Crawford Hill Lab on the characterization of advanced lasers, optical access networks, and data-over-cable access protocols. He was with Lucent Technologies as it was spun out of AT&T in 1996, where he was the Head of the Access Research Department, and managed the R&D of passive optical network systems and cable modem head end equipment. In 2000, he returned to AT&T, where he is currently the Executive Director, Optical Systems Research, and is engaged with advancing fiber communication technologies for the entire network (intercity, metro, and access), including 100 Gb/s transmission systems and dynamic wavelength networks. Since 2007, he has also been working on assessing, with a goal of reducing AT&T's electricity consumption.

Milorad Cvijetic, photograph and biography not available at the time of publication.

Lynn Nelson, photograph and biography not available at the time of publication.

Martin Birk, photograph and biography not available at the time of publication.

Guodong Zhang, photograph and biography not available at the time of publication.

S. Ten, photograph and biography not available at the time of publication.

H. B. Matthew, photograph and biography not available at the time of publication.

S. K. Mishra, photograph and biography not available at the time of publication.